LETTERS
PUBLISHED ONLINE: 19 JANUARY 2015 | DOI: 10.1038/NNANO.2014.308
nature nanotechnology

Ultralow-threshold electrically injected AlGaN nanowire ultraviolet lasers on Si operating at low temperature

K. H. Li, X. Liu, Q. Wang, S. Zhao and Z. Mi*

Ultraviolet laser radiation has been adopted in a wide range of applications as diverse as water purification, flexible displays, data storage, sterilization, diagnosis and bioagent detection[1–3]. Success in developing semiconductor-based, compact ultraviolet laser sources, however, has been extremely limited. Here, we report that defect-free disordered AlGaN core–shell nanowire arrays, formed directly on a Si substrate, can be used to achieve highly stable, electrically pumped lasers across the entire ultraviolet AII (UV-AII) band (~320–340 nm) at low temperatures. The laser threshold is in the range of tens of amps per centimetre squared, which is nearly three orders of magnitude lower than those of previously reported quantum-well lasers[4–6]. This work also reports the first demonstration of electrically injected AlGaN-based ultraviolet lasers monolithically grown on a Si substrate, and offers a new avenue for achieving semiconductor lasers in the ultraviolet B (UV-B) (280–320 nm) and ultraviolet C (UV-C) (<280 nm) bands.

Compared with the conventional excimer ultraviolet lasers or frequency doubled/tripled solid-state lasers, AlGaN-based ultraviolet devices offer an enormous number of advantages, which include high efficiency, small size and low power consumption. Progress in this field, however, has been severely limited by the large dislocation densities and residual strain introduced during the growth of AlGaN epitaxial layers, which can induce wafer bowing and cracking and lead to unacceptably high optical cavity loss. Consequently, the operation wavelengths of electrically injected ultraviolet laser diodes have been limited to the ultraviolet AI band (~340–400 nm), with the threshold current density in the range of 10,000 A cm^{-2} or higher[4–10], in spite of intensive studies on improving the optical gain of AlGaN with a high Al content[11–15]. Alternatively, nearly defect-free single-nanowire laser[16,17] or nanowire laser arrays[18–22] have been investigated extensively. Owing to the complicated fabrication and/or growth process, an electrically injected nanowire ultraviolet laser has hitherto not been realized, severely limiting their practical applications. Here, by exploiting the Anderson localization of light[23–25] in self-organized AlGaN/GaN nanowire heterostructures spontaneously formed on the Si substrate, we demonstrate ultralow-threshold lasing in the entire UV-AII band, the shortest wavelengths ever reported for any electrically injected semiconductor lasers. Such a lithography-free process for fabricating defect-free nanowire laser arrays on large-area Si substrates provides many attractive advantages, including low cost and ultralow power consumption, and enables a new generation of electrically injected semiconductor lasers with operation wavelengths far beyond those previously possible.

Anderson localization relies on the use of multiple scattering in a random cavity. The challenges in the implementation in practical devices are directly related to the fabrication of such optical cavities in a low-cost, scalable and controllable process[26–30]. In this work, we first studied the design of lithography-free disordered nanowire arrays required for a stable lasing operation in the UV-AII band, schematically shown in Fig. 1a, and we further show that these requirements can be achieved readily by self-organized AlGaN nanowire arrays formed on a Si substrate using radiofrequency plasma-assisted molecular beam epitaxy (MBE). It is known that the formation of high-quality factor (Q) random lasing is strongly related to the strength of light localization in the random cavity system, which is governed by the orientation, size and filling fraction of the nanostructures[26]. For a vertically aligned, randomly distributed, subwavelength-scale nanowire array, the density of nanowires plays a crucial role in sustaining a random lasing action. The low density of nanowire structures would not support random lasing, and the scattering mean free path has to be optimized. We performed a detailed two-dimensional (2D) simulation to identify the dependence of the optical resonance (wavelength ~330 nm) on the nanowire diameter and filling factor, as shown in Fig. 1b (also see Supplementary Section 1). In this simulation, a 15% diameter variation is assumed, based on the typical variations of self-organized GaN nanowire structures. The probabilities of forming a high-Q cavity versus the average nanowire diameter and filling factor are shown in Fig. 1b. It is clear that high-Q cavities can form with a high probability in disordered nanowire arrays with average diameters of ~70–75 nm and filling factors of ~30%. Such randomly distributed nanowires mimic the configuration obtained by self-organized nanowire arrays directly on the Si substrate, described below. The simulated profile of the mode in one random cavity with Q as high as 20,000 is shown in Fig. 1c.

To achieve optical confinement along the vertical direction, AlGaN nanowire double-heterostructures were designed. Schematically shown in Fig. 1d, the undoped AlGaN active region is sandwiched between n-AlGaN and p-AlGaN cladding layers. The thicknesses of the AlGaN active region and the n-AlGaN and p-AlGaN layers are ~50, 150 and 150 nm, respectively. The average Al compositions in the active region and cladding layers are estimated to be in the range ~30% and 56%, respectively (see Supplementary Section 2). Such AlGaN nanowire double-heterostructures were grown on Si-doped GaN nanowire templates on an n-type Si(111) substrate by MBE without using any external metal catalyst (see Methods). A thin (~25 nm) GaN:Mg layer was grown as the top contact layer. The nanowire heterostructures exhibit strong photoluminescence (PL) emission at room temperature, shown in Fig. 1e. Extensive growth optimization was

Department of Electrical and Computer Engineering, McGill University, 3480 University Street, Montreal, Quebec H3A 0E9, Canada.
*e-mail: zetian.mi@mcgill.ca

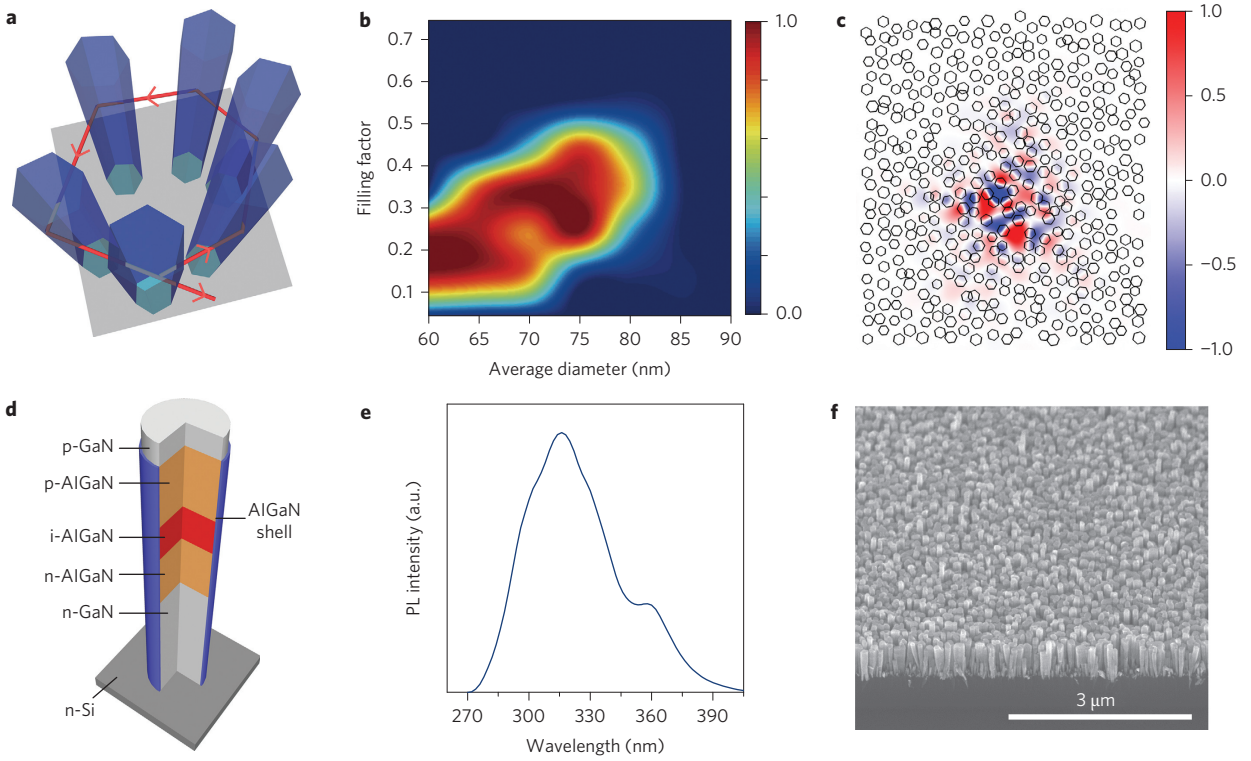

Figure 1 | Simulation of AlGaN nanowire random cavity, and optical and structural characterization. a, Schematic diagram illustrating the formation of a closed-loop path inside AlGaN nanowire arrays; red arrows denote the photon path. **b**, Probability of forming a high-*Q* cavity versus filling factors and diameters of nanowires. **c**, Simulation result showing the profile of the electric field $E_{||c\text{-axis}}$ for a high-*Q* cavity; black hexagons represent spontaneously formed nanowires. **d**, Schematic of AlGaN nanowire double-heterostructures. **e**, PL spectrum measured at room temperature. **f**, A 45° tilted SEM image of nanowire arrays grown on a Si substrate.

performed to achieve AlGaN nanowire arrays that can meet the aforementioned design requirements, in terms of both the nanowire diameter and filling factor. Structural properties of such nanowire arrays are first characterized by scanning electron microscopy (SEM). Shown in Fig. 1f is an SEM image taken at a 45° angle. It is seen that the nanowires are aligned vertically on the Si substrate and exhibit a high degree of size and height uniformity. The average filling factor is expected to be smaller than it appears in the SEM image because of the tapered nanowire morphology (described below). More detailed studies further confirm that the average spacing between nanowires is much less than the emission wavelength, and thus enables recurrent multiple scattering inside nanowires (see Supplementary Section 4).

We further performed structural studies of AlGaN nanowire double-heterostructures by transmission electron microscopy (TEM). A high-resolution TEM image taken from the interface between the p-AlGaN cladding layer and the p-GaN contact layer is shown in Fig. 2a. It is clear that both the p-AlGaN and p-GaN regions are free of stacking faults and misfit dislocations. More importantly, a sharp heterointerface can be clearly observed. Detailed high-resolution TEM studies further confirm that the whole AlGaN nanowire is free of extended defects and dislocations. Elemental mapping was carried out in the scanning transmission electron microscopy (STEM) mode. Illustrated in Fig. 2b is a high-angle annular dark field (HAADF) image, which clearly shows that the nanowire is inversely tapered, that is, the diameter increases along the growth direction and becomes nearly constant in the top region. Consequently, this leads to a strong photon confinement in the active region of the nanowire laser structures and any optical loss through the Si substrate is greatly minimized (see Supplementary Section 3). Al and Ga element mapping is shown in Fig. 2c in pseudo colours, with the mapping region marked in Fig. 2b. It is clear that in the active region the Ga content is increased whereas the Al content is decreased. This Al/Ga composition change is further confirmed by the energy-dispersive X-ray spectrometry (EDXS) line scan across the active region along the axial direction, illustrated in Fig. 2d. In addition, the EDXS line scan across the active region but along the radial direction indicates the presence of Al-rich AlGaN shells (Fig. 2e). Such a spontaneous formation of Al-rich AlGaN shells can be ascribed to the much slower Al adatom migration compared to that of Ga adatoms. The enhanced Al composition in the near-surface region can lead to a strong carrier confinement, and thereby significantly reduce nonradiative surface recombination and enhance the carrier-injection efficiency in the active region of the nanowire laser[31].

Subsequently, nanowire light-emitting devices were fabricated using standard photolithography, surface passivation and planarization, and contact-metallization techniques (see Methods). The current–voltage characteristics are shown in Fig. 3a, and a very low leakage current under a reverse bias is indicated in the inset. The lasing characteristics of AlGaN nanowires were investigated by electrical injection under a continuous-wave operation at various temperatures. Figure 3b shows the electroluminescence (EL) spectra of AlGaN nanowire devices measured at 6 K. Under varying current densities, it was observed that sharp peaks were superimposed on the broad spontaneous emission background of the AlGaN active region. Two discrete peaks centred at 332.7 nm and 334.1 nm were measured. As the latter peak is clearly dominant, its threshold and linewidth properties were analysed (analysis of the lasing peak at 332.7 nm is shown in Supplementary Section 6). Figure 3c,d show

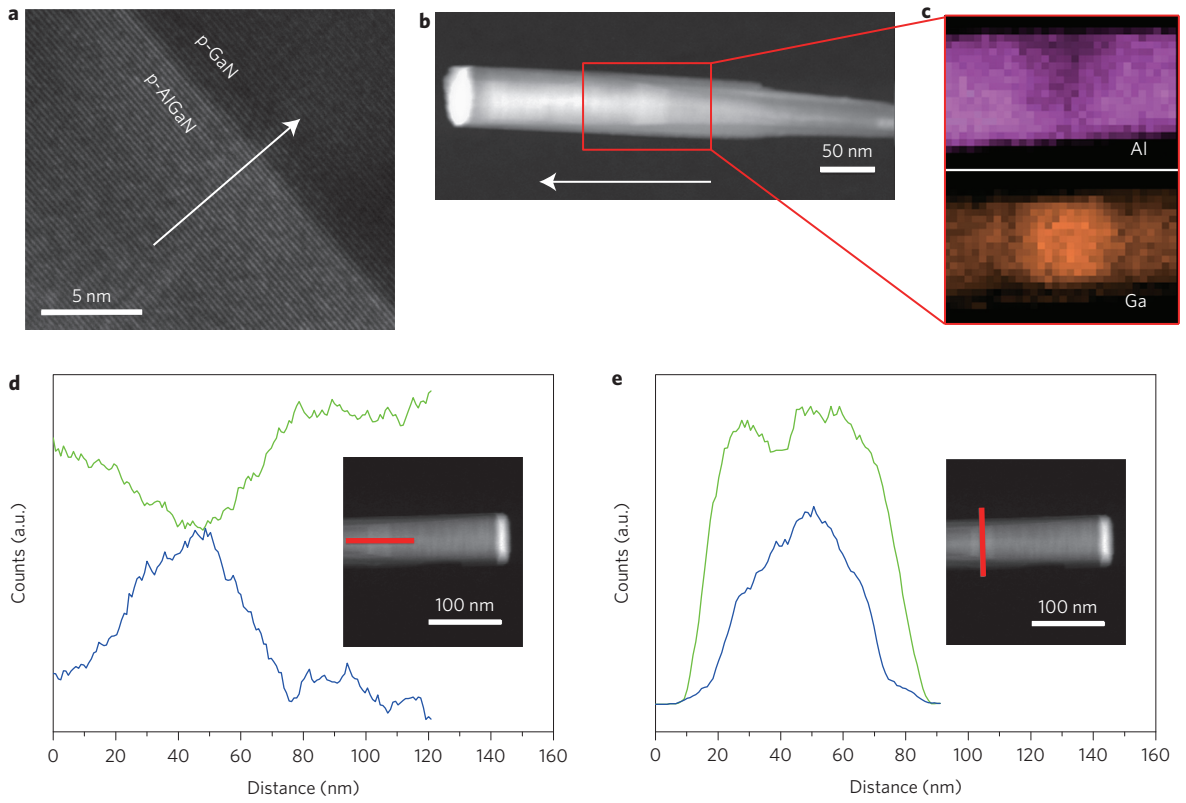

Figure 2 | Characterization of a single AlGaN nanowire. a, High-resolution TEM image taken from the interface between a p-AlGaN cladding layer and a p-GaN contact layer. The arrow indicates the nanowire growth direction. The dark region corresponds to p-GaN and the bright region corresponds to p-AlGaN. **b**, HAADF image of a single AlGaN nanowire. The arrow indicates the growth direction. **c**, Al and Ga element mapping for the selected region in **b**. It is clear that in the active region the Ga content is increased, whereas the Al content is decreased. **d**, The EDXS line scan across the active region along the axial direction shows the Al (green curve) and Ga (blue curve) compositional changes in the active region. **e**, The EDXS line scan along the radial direction of the active region indicates the presence of Al-rich AlGaN shells (Al, green curve; Ga, blue curve). The red lines in the insets of **d** and **e** denote where the EDXS line scans were performed.

the plots of the integrated intensity and linewidth of the dominant peak as a function of the current density, respectively. A nonlinear increase of the emission intensity and spectral narrowing near the threshold provides unambiguous evidence for the achievement of lasing. At the lasing threshold, the spectral linewidth is as narrow as 0.2 nm, which is limited by the spectral resolution of the set-up. The lasing threshold is estimated to be ~12 A cm^{-2}, which was derived by taking into account the nanowire structure, filling factor and active lasing area (~10 μm × 10 μm). It is nearly three orders of magnitude lower than those of previously reported GaN-based ultraviolet lasers[4–6]. The output power is estimated to be ~2 μW at an injection current of 30 A cm^{-2}. Figure 3e shows the plot of peak positions as a function of current densities. It was observed that the lasing wavelengths remain virtually unchanged when the injection current increases from threshold to ~6 times above threshold, which suggests that the lasing emission is dominated by the extremely stable excitonic transition rather than by the emission related to electron–hole plasma. The ultralow threshold is attributed to the high-*Q* optical resonance, the nearly defect-free AlGaN nanowires, the drastically reduced nonradiative surface recombination offered by the AlGaN core–shell structures and possibly the strong quantum-confinement effect related to the nanometric compositional fluctuations of the active region[32,33].

Temperature-dependent measurements were also carried out for a fixed current density of ~27 A cm^{-2}. When the temperature rises from 6 to 100 K, both discrete sharp peaks exhibit redshifts of ~0.7 nm, shown in Fig. 3f. The redshift can be attributed to two main factors. With the increase in temperature, the bandgap shrinkage of the AlGaN active region gives rise to a peak-gain shift. The other contributing factor is related to the refractive index change inside the random cavities because of the thermal effect. Analysis of the lasing performance at various temperatures is described in Supplementary Section 7.

As shown in the detailed modelling, the resonance cavity formed by disordered nanowire arrays can be tuned by rational design of the nanowire structures. In this regard, we performed extensive measurements and observed ultralow-threshold lasing in various device structures (see Supplementary Section 9). The emission wavelength can be tuned across the entire ultraviolet-AII band (~320 nm to 340 nm), the shortest wavelength ever reported for an electrically injected semiconductor laser. Also, we performed analyses that further confirmed the measured ultralow-threshold lasing was not caused by lasing from single nanowires (see Supplementary Section 8).

In summary, we have demonstrated that AlGaN core–shell nanowires can function as highly scattered random media to support a closed-loop mode by recurrent multiple scattering, which leads to ultralow-threshold electrically injected lasers in the wavelength range of ~320 to 340 nm on a Si substrate. This study effectively connects the concept of the Anderson localization of light and the self-organized formation of nanowires and provides a viable approach for the practical implementation of the elegant concept of random lasers in a low-cost, scalable and controllable process. It is expected that by further tuning the nanowire parameters, ultralow-threshold nanowire lasers across the entire UV-A, -B and -C spectral ranges could be achieved on a Si substrate for biochemical, sensing, communication and lighting applications.

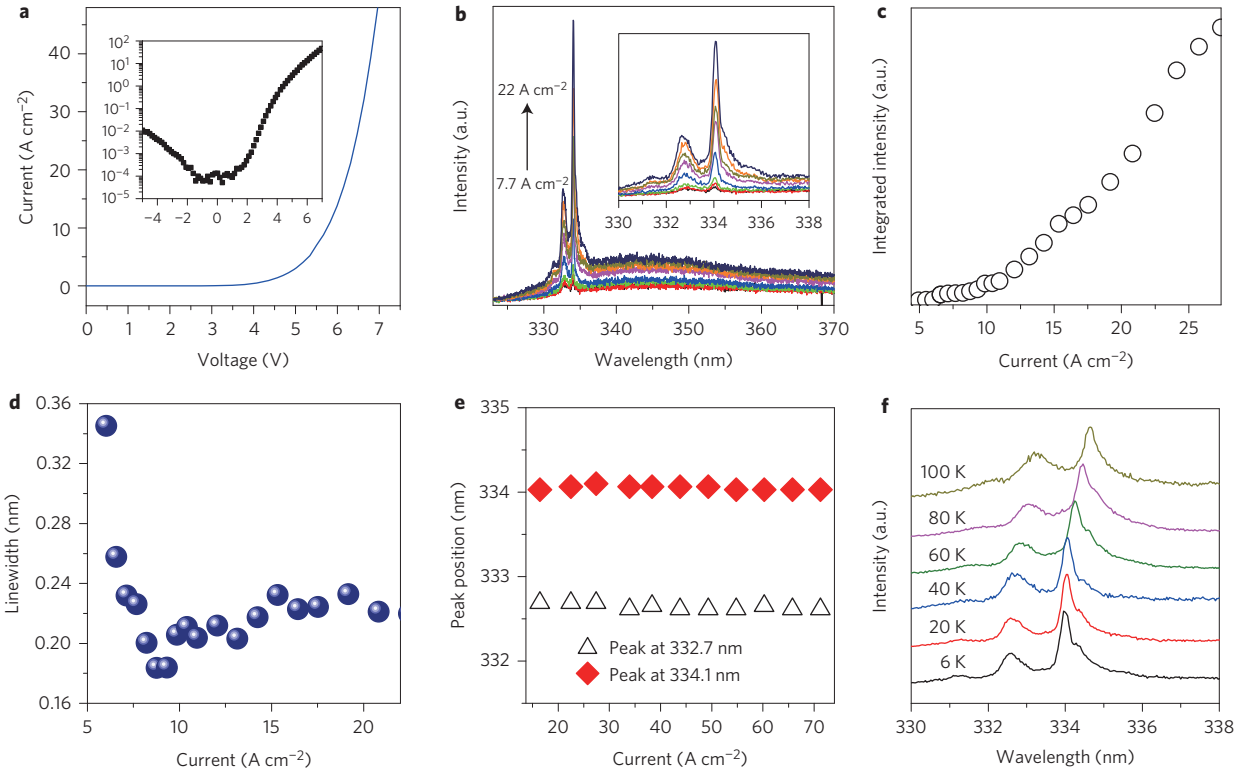

Figure 3 | Device performance and characterization. a, *I–V* characteristics of the AlGaN nanowire laser; the inset shows the *I–V* curve on a semi-log scale. **b**, Emission spectra measured at 6 K under different current densities. The black arrow denotes that the current density increases from 7.7 A cm^{-2} to 22 A cm^{-2} and the inset shows an enlarged view of the lasing spectra. **c**,**d**, Integrated intensity (**c**) and linewidth (**d**) of the lasing peak at 334.1 nm as a function of injection-current density. **e**, Plot of peak position versus current density. **f**, EL spectra measured at different operation temperatures.

Methods

Nanowire laser design and simulation. Given that the nanowire diameter and operation wavelength are much smaller than the nanowire length, a 2D simulation was performed to find out the probability of forming a high-*Q* random cavity for AlGaN nanowire arrays. In this study, the nanowires were considered to be hexagonal. The crucial parameters for a random nanowire array are the average diameter *d* and the filling factor. The diameters were distributed randomly with a lower limit of 0.85*d* and an upper limit of 1.15*d*. The positions of the nanowires were also assumed to be distributed randomly. For any given combination of average nanowire diameter and filling factor, about 200 random nanowire arrays were generated and the possible modes around 330 nm were computed by the RF module of Comsol Multiphysics 4.3b. The optimal combination of filling factor and average diameter to achieve high-*Q* cavity modes was finally obtained, and provided guidance for the subsequent growth and characterization of nanowire laser structures.

Molecular beam epitaxial growth. In this study, catalyst-free, vertically aligned AlGaN nanowire double-heterostructures were grown on two inch (5 cm) n-Si(111) substrates by a Veeco Gen II MBE system equipped with a radiofrequency plasma-assisted nitrogen source under nitrogen-rich conditions. Prior to the growth, the oxide on the Si surface was removed by hydrofluoric acid (10%) and further thermally cleaned *in situ* at ~770 °C. The RHEED (reflection high-energy electron diffraction) pattern of the Si substrate prior to nanowire growth is shown in Supplementary Section 2 (Supplementary Fig. 2a). During the growth process, the nitrogen flow rate was kept at 1.0 standard cubic centimetre per minute, with a forward plasma power of ~350 W. GaN nanowires were grown at ~750 °C, and the AlGaN cladding segments and active region were grown at relatively high temperatures of 800 °C. The active region and p- and n-cladding layers were grown with Al beam equivalent pressures (BEPs) of ~1.30×10^{-8} Torr and ~3.93×10^{-8} Torr, respectively, with a constant Ga BEP of ~2.75×10^{-8} Torr. The Si-doping level in the n-cladding layer was estimated to be ~5×10^{17} cm^{-3}.

Structural characterization. The SEM images were taken using a Hitachi S-4700 system. The experiments were performed with a 45° angle. An accelerating voltage of 10 kV and a current of 10 μA were used for imaging. The detector was cooled with liquid nitrogen. HAADF and EDXS were performed in the STEM mode of a Tecnai G^2 F20 S/TEM system, which was equipped with a Gatan 4 k × 4 k CCD (charge-coupled device) camera. The operation voltage was 200 kV. The cold finger was cooled with liquid nitrogen to avoid contamination. Curve smoothing was performed for the EDXS data.

Device fabrication. The electrically injected devices were fabricated using standard microfabrication procedures. Prior to the deposition of metal contacts, the air voids between adjacent nanowires were filled with polyimide to isolate the p- and n-type faces electrically. The top p-type surfaces of the nanowires were exposed by the etch-back process using oxygen plasma. The mesa region was then defined by the photolithography process, and p- and n-contacts were deposited using an e-beam evaporator followed by rapid thermal annealing at 550 °C for one minute. A detailed fabrication process flow is shown in Supplementary Section 5.

Device characterization. PL measurements were carried out at room temperature using a 266 nm diode-pumped solid-state laser. For the EL measurement, the wire-bonded device was mounted inside the cryostat with the quartz top cover and the cooling system was fixed on a motorized *x–y* stage (Aerotech's ANT130-XY-ULTRA), which provided precise mapping over about a 10 × 10 μm^2 lasing region. The emitted signals were collected by an ultraviolet objective and detected by a liquid-nitrogen cooled CCD attached to a 550 mm spectrograph with 1,200 grooves per millimetre, which offered a spectral resolution of ~0.14 nm. The temperature-dependent measurements were performed in a temperature-controlled liquid helium cryostat.

Received 4 July 2014; accepted 19 November 2014; published online 19 January 2015

References

1. Lindenauer, K. G. & Darby, J. L. Ultraviolet disinfection of wastewater: effect of dose on subsequent photoreactivation. *Water Res.* **28,** 805–817 (1994).
2. Chwirot, B. W. *et al.* Ultraviolet laser-induced fluorescence of human stomach tissues: detection of cancer tissues by imaging techniques. *Lasers Surg. Med.* **21,** 149–158 (1997).
3. Ramanujam, P. S. & Berg, R. H. Photodimerization in dipeptides for high capacity optical digital storage. *Appl. Phys. Lett.* **85,** 1665–1667 (2004).
4. Yoshida, H., Yamashita, Y., Kuwabara, M. & Kan, H. Demonstration of an ultraviolet 336 nm AlGaN multiple-quantum-well laser diode. *Appl. Phys. Lett.* **93,** 241106 (2008).

5. Kneissl, M., Treat, D. W., Teepe, M., Miyashita, N. & Johnson, N. M. Ultraviolet AlGaN multiple-quantum-well laser diodes. *Appl. Phys. Lett.* **82,** 4441–4443 (2003).
6. Yoshida, H., Yamashita, Y., Kuwabara, M. & Kan, H. A 342-nm ultraviolet AlGaN multiple-quantum-well laser diode. *Nature Photon.* **2,** 551–554 (2008).
7. Iida, K. *et al.* 350.9 nm UV laser diode grown on low-dislocation-density AlGaN. *Jpn. J. Appl. Phys.* **43,** L499 (2004).
8. Masui, S. *et al.* 365 nm ultraviolet laser diodes composed of quaternary AlInGaN alloy. *Jpn. J. Appl. Phys.* **42,** L1318 (2003).
9. Yoshida, H., Takagi, Y., Kuwabara, M., Amano, H. & Kan, H. Entirely crack-free ultraviolet GaN/AlGaN laser diodes grown on 2-in. sapphire substrate. *Jpn. J. Appl. Phys.* **46,** 5782 (2007).
10. Haeger, D. A. *et al.* 384 nm laser diode grown on a $(20\bar{2}1)$ semipolar relaxed AlGaN buffer layer. *Appl. Phys. Lett.* **100,** 161107 (2012).
11. Guo, W. *et al.* Stimulated emission and optical gain in AlGaN heterostructures grown on bulk AlN substrates. *J. Appl. Phys.* **115,** 103108 (2014).
12. Francesco Pecora, E. *et al.* Sub-250 nm light emission and optical gain in AlGaN materials. *J. Appl. Phys.* **113,** 013106 (2013).
13. Zhang, J., Zhao, H. & Tansu, N. Effect of crystal-field split-off hole and heavy-hole bands crossover on gain characteristics of high Al-content AlGaN quantum well lasers. *Appl. Phys. Lett.* **97,** 111105 (2010).
14. Zhang, J., Zhao, H. & Tansu, N. Large optical gain AlGaN-delta-GaN quantum wells laser active regions in mid- and deep-ultraviolet spectral regimes. *Appl. Phys. Lett.* **98,** 171111 (2011).
15. Park, S-H. Optical gain characteristics of non-polar Al-rich AlGaN/AlN quantum well structures. *J. Appl. Phys.* **110,** 063105 (2011).
16. Gradečak, S., Qian, F., Li, Y., Park, H-G. & Lieber, C. M. GaN nanowire lasers with low lasing thresholds. *Appl. Phys. Lett.* **87,** 173111 (2005).
17. Johnson, J. C. *et al.* Single gallium nitride nanowire lasers. *Nature Mater.* **1,** 106–110 (2002).
18. Xu, H. *et al.* Single-mode lasing of GaN nanowire-pairs. *Appl. Phys. Lett.* **101,** 113106 (2012).
19. Heo, J., Jahangir, S., Xiao, B. & Bhattacharya, P. Room-temperature polariton lasing from GaN nanowire array clad by dielectric microcavity. *Nano Lett.* **13,** 2376–2380 (2013).
20. Wu, C. Y. *et al.* Plasmonic green nanolaser based on a metal-oxide-semiconductor structure. *Nano Lett.* **11,** 4256–4260 (2011).
21. Kouno, T., Kishino, K., Suzuki, T. & Sakai, M. Lasing actions in GaN tiny hexagonal nanoring resonators. *IEEE Photon. J.* **2,** 1027–1033 (2010).
22. Frost, T. *et al.* Monolithic electrically injected nanowire array edge-emitting laser on (001) silicon. *Nano Lett.* **14,** 4535–4541 (2014).
23. Painter, O. *et al.* Two-dimensional photonic band-gap defect mode laser. *Science* **284,** 1819–1821 (1999).
24. Matsubara, H. *et al.* GaN photonic-crystal surface-emitting laser at blue–violet wavelengths. *Science* **319,** 445–457 (2008).
25. Sakai, M. *et al.* Random laser action in GaN nanocolumns. *Appl. Phys. Lett.* **97,** 151109 (2010).
26. Yu, S. F., Yuen, C., Lau, S. P., Park, W. I. & Yi, G-C. Random laser action in ZnO nanorod arrays embedded in ZnO epilayers. *Appl. Phys. Lett.* **84,** 3241–3243 (2004).
27. Liu, C. Y. *et al.* Electrically pumped near-ultraviolet lasing from ZnO/MgO core/shell nanowires. *Appl. Phys. Lett.* **99,** 063115 (2011).
28. Liu, X. Y., Shan, C. X., Wang, S. P., Zhang, Z. Z. & Shen, D. Z. Electrically pumped random lasers fabricated from ZnO nanowire arrays. *Nanoscale* **4,** 2843–2846 (2012).
29. Chu, S. *et al.* Electrically pumped waveguide lasing from ZnO nanowires. *Nature Nanotech.* **6,** 506–510 (2011).
30. Lo, M-H., Cheng, Y-J., Liu, M-C., Kuo, H-C. & Wang, S. C. Lasing at exciton transition in optically pumped gallium nitride nanopillars. *Opt. Express* **19,** 17960–17965 (2011).
31. Nguyen, H. P. T. *et al.* Breaking the carrier injection bottleneck of phosphor-free nanowire white light-emitting diodes. *Nano Lett.* **13,** 5437–5442 (2013).
32. Sampath, A. V. *et al.* Growth of AlGaN containing nanometer scale compositional inhomogeneities for ultraviolet light emitters. *J. Vac. Sci. Technol. B* **29,** 03C134 (2011).
33. Pierret, A., Bougerol, C., Gayral, B., Kociak, M. & Daudin, B. Probing alloy composition gradient and nanometer-scale carrier localization in single AlGaN nanowires by nanocathodoluminescence. *Nanotechnology* **24,** 305703 (2013).

Acknowledgements

This work was supported by the Natural Sciences and Engineering Research Council of Canada and US Army Research Office under Grant W911NF-12-1-0477. Part of the work was performed in the McGill University Micro Fabrication Facility.

Author contributions

K.H.L. fabricated the devices and carried out the experimental measurements. X.L. performed the device design and contributed to the theoretical calculations, device fabrication and measurements. K.H.L. and X.L. made equal contributions. S.Z. conducted the MBE growth of nanowires and contributed to the TEM analysis. Q.W. contributed to the preliminary works on device characteristics. Z.M. conceived the experiments and supervised and led the project. The paper was written by K.H.L. and Z.M. with contributions from the other authors.

Additional information

Supplementary information is available in the online version of the paper. Reprints and permissions information is available online at www.nature.com/reprints. Correspondence and requests for materials should be addressed to Z.M.

Competing financial interests

The authors declare no competing financial interests.